Effective Inclusion of Mechanical and Electrical Anharmonicity in Excited Electronic States: VPT2-TDDFT Route

Franco Egidi,[⊥,†] David B. Williams-Young,[‡,⊥] Alberto Baiardi,[†,⊥] Julien Bloino,[§] Giovanni Scalmani,[∥] Michael J. Frisch,[∥] Xiaosong Li,*[‡] and Vincenzo Barone*[†]

[†]Scuola Normale Superiore, Piazza dei Cavalieri 7, 56126 Pisa, Italy
[‡]Department of Chemistry, University of Washington, Seattle, Washington 98195, United States
[§]Consiglio Nazionale delle Ricerche, Istituto di Chimica dei Composti OrganoMetallici (ICCOM-CNR), UOS di Pisa, Area della Ricerca CNR, Via G. Moruzzi 1, Pisa 56124, Italy
[∥]Gaussian, Inc., 340 Quinnipiac St., Bldg. 40, Wallingford, Connecticut 06492, United States

S Supporting Information

ABSTRACT: We present a reliable and cost-effective procedure for the inclusion of anharmonic effects in excited-state energies and spectroscopic intensities by means of second-order vibrational perturbation theory. This development is made possible thanks to a recent efficient implementation of excited-state analytic Hessians and properties within the time-dependent density functional theory framework. As illustrated in this work, by taking advantage of such algorithmic developments, it is possible to perform calculations of excited-state infrared spectra of medium-large isolated molecular systems, with anharmonicity effects included in both the energy and property surfaces. We also explore the use of this procedure for the inclusion of anharmonic effects in the simulation of vibronic bandshapes of electronic spectra and compare the results with previous, more approximate models.
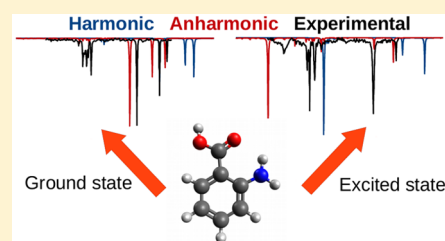
1. INTRODUCTION

Molecular spectroscopy has become the method of choice for the study of all types of molecular systems, from small isolated molecules to large supramolecular clusters in complex environments. Experimental breakthroughs have made the use of spectroscopic techniques routinely available for both science and industry, while parallel theoretical and computational developments have proved to be of great help in the interpretation of experimental results, as well as suitable substitutes in the investigation of novel systems thanks to their predictive powers. After decades of theoretical work and computational effort, the field has reached a certain level of maturity for medium-sized isolated molecules in the ground state, for which spectroscopic responses of high order can be simulated, from simple one-photon absorption to resonance Raman optical activity.[1,2] The accuracy of a computed vibrational spectrum rests not only on an appropriate choice of the underlying electronic structure method (whether it be a choice of functional in density functional theory (DFT) or wave function theory model) and basis set but also on the level of theory chosen to describe the potential energy surface (PES). The harmonic approximation is usually used for PES and the property that induces the spectroscopic response (i.e., the electric dipole moment for infrared absorption) also truncated to the lowest order. It has however been shown that the inclusion of anharmonic effects can be crucial for the simulation of accurate vibrational spectra[3–5] and to include vibrational effects in the calculation of response properties.[6–11] Anharmonic effects have been extensively studied for molecules in the ground electronic

state; however, spectroscopic properties in excited electronic states are much less known. In line with our efforts to develop computational tools for the simulation of spectroscopic properties of molecular systems,[12,13] in this contribution we fill this gap by presenting the first fully anharmonic excited-state infrared spectra calculated by means of second-order vibrational perturbation theory (VPT2).[14–20] VPT2 has been extensively used in the past for predicting ground-state vibrational zero-point energies and thermodynamic properties,[21] as well as vibrational spectra including infrared absorption, vibrational circular dichroism,[5,12] Raman,[5] hyper-Raman,[22] and Raman optical activity,[23] with anharmonicity effects being included in both the force field and the property surface (mechanical and electric anharmonicities, respectively). To develop a computationally efficient method to include anharmonicity effects for excited states of medium-large molecules, an indispensable ingredient is the availability of analytical Hessians and property first derivatives, which can be further numerically differentiated to yield the anharmonic force constants. Thanks to recent developments,[24–28] it is now possible to perform these calculations with the inclusion of both electrical and mechanical anharmonicities in the spectra. In addition, being able to model both ground and excited state potential energy surfaces at the anharmonic level allows for a more accurate prediction of vibronic couplings which are responsible for the vibronic band shape in electronic

absorption and emission spectra.[29−35] In the following sections, we recall the theoretical basis of the methodology, then present a few applications of the method.

2. THEORY AND IMPLEMENTATION

2.1. Analytical TDDFT Second Derivatives. Various developments have been carried out in recent years which have led to improvements in ab initio methods needed to perform VPT2 calculations, which require both high-order energy and property derivatives. For the ground state, analytic formulas and implementations of cubic and quartic force constants have been proposed in the literature at the Hartree−Fock (HF) and DFT levels.[36−40] The recent development of analytical second-order geometrical derivatives of excitation energies obtained using the time-dependent density functional theory (TDDFT) and its Tamm−Dancoff approximation (TDA)[24−28] was instrumental in extending computational spectroscopic techniques commonly employed for molecules in the ground electronic state to electronically excited systems. In particular, the proper treatment of frozen-core and frozen-virtual orbitals and an efficient approach to QM/MM systems including electrostatic embedding has made it possible to obtain analytical excitation energy first and second derivatives for very large systems (>3000 atoms).[28]

The application of VPT2 for studies of excited state molecular vibrations requires the excited state energy third- and fourth-derivatives (cubic and quartic terms). However, an implementation of the analytical TDDFT third- and fourth-derivatives is impractical because it requires the very high order (up to sixth) of the exchange-correlation functional derivatives whose stabilities can be a challenge even at the second order. With the availability of the excited state analytical Hessian, higher order derivatives of the excited state energy can be computed using the finite difference method which also avoids explicit computations of high-order exchange-correlation functional derivatives.

2.2. Excited-State Anharmonic Force Field. Using the excited-state analytic second derivatives of the potential energy, it is possible to build the cubic and semi-diagonal quartic force constants necessary to compute the vibrational energies at the VPT2 level by numerical differentiation, in the same way as is now commonly done for the ground state

$$
k_{ijk} = \frac{\partial^3 V}{\partial q_i \partial q_j \partial q_k} = \frac{1}{3} \Bigg[\sqrt{\frac{\hbar}{2\pi c \omega_i}} \frac{k_{jk}(+\delta Q_i) - k_{jk}(-\delta Q_i)}{2\delta Q_i}
$$
$$
+ \sqrt{\frac{\hbar}{2\pi c \omega_j}} \frac{k_{ik}(+\delta Q_j) - k_{ik}(-\delta Q_j)}{2\delta Q_j}
$$
$$
+ \sqrt{\frac{\hbar}{2\pi c \omega_k}} \frac{k_{ij}(+\delta Q_k) - k_{ij}(-\delta Q_k)}{2\delta Q_k} \Bigg]
$$
(1)

$$
k_{iijk} = \frac{\partial^4 V}{\partial q_i^2 \partial q_j \partial q_k} = \frac{\hbar}{2\pi c \omega_i} \frac{k_{jk}(+\delta Q_i) - k_{jk}(-\delta Q_i)}{\delta Q_i^2}
$$

$$
k_{iijj} = \frac{\partial^4 V}{\partial q_i^2 \partial q_j^2} = \frac{1}{2} \Bigg[\frac{\hbar}{2\pi c \omega_i} \frac{k_{jj}(+\delta Q_i) - k_{jj}(-\delta Q_i)}{\delta Q_i^2}
$$
$$
+ \frac{\hbar}{2\pi c \omega_j} \frac{k_{ii}(+\delta Q_j) - k_{ii}(-\delta Q_j)}{\delta Q_j^2} \Bigg]
$$
(2)

with Q the vector of mass-weighted normal coordinates, ω the vector of harmonic wavenumbers, and k the matrix of second derivatives of the potential energies with respect to the dimensionless (q) normal coordinates.

The energy of a vibrational state of $|m\rangle$ (in cm^{-1}) is given by

$$
\varepsilon_m = \varepsilon_0 + \sum_{i=1}^{N} v_i^m \omega_i + \sum_{i,j=1}^{N} \chi_{ij} \left[v_i^m v_j^m + \frac{1}{2}(v_i^m + v_j^m) \right]
$$
(3)

where v_i^m is the number of quanta associated with mode i in state m, ε_0 is the zero-point vibrational energy, and χ is the matrix containing the anharmonic contribution (see refs 41 and 42 for the definition of ε_0 and χ).

At the VPT2 level, not considering variational corrections, any vibrational transition energy within a given electronic state can be easily computed from eq 3. Formulas for the transition from the ground state to fundamentals, first overtones, and 2-state combinations are reported below,

Fundamental bands

$$
|1_i\rangle \rightarrow \nu_{1_i} = \omega_i + 2\chi_{ii} + \frac{1}{2} \sum_{j \neq i} \chi_{ij}
$$

Overtones

$$
|2_i\rangle \rightarrow \nu_{2_i} = 2\omega_i + 6\chi_{ii} + \sum_{j \neq i} \chi_{ij} = 2\nu_{1_i} + 2\chi_{ii}
$$

Combination bands

$$
|1_i 1_j\rangle \rightarrow \nu_{1_i 1_j} = \omega_i + \omega_j + 2(\chi_{ii} + \chi_{jj} + \chi_{ij})
$$
$$
+ \frac{1}{2} \sum_{k \neq i,j} \{\chi_{ik} + \chi_{jk}\} = \nu_{1_i} + \nu_{1_j} + \chi_{ij}
$$

Similarly, provided that analytical first derivatives of the properties of interest are available, it is possible to compute the second and semi-diagonal third derivatives necessary to obtain the anharmonic intensities through numerical differentiation as well. An additional difficulty here is the absence of a unique and compact formula applicable to every transition, and the most effective form will depend on the initial and final states. Formulas for transitions from the ground state up to 3 quanta can be found in ref 41.

At variance, the computational cost of a full anharmonic treatment for the simulation of vibronic spectra, even at the VPT2 level, is too high but for the smallest molecules.[43,44] Consequently, an alternative, more affordable way is needed to deal with medium-to-large molecular systems. The approach adopted here is to focus on the band positions. Following eq 3, the transition energy between vibronic states $|\bar{i}\rangle$ and $|\bar{\bar{f}}\rangle$ (the single overbar refers to the initial electronic state and the double bar to the final one) is

$$
\Delta \varepsilon_{if} = \Delta E_{el} + \bar{\bar{\varepsilon}}_0 - \bar{\varepsilon}_0 + \sum_{k=1}^{N} (v_k^f \bar{\bar{\omega}}_k - v_k^i \bar{\omega}_k)
$$
$$
+ \sum_{k,l=1}^{N} \left(\bar{\bar{\chi}}_{kl} \left[v_k^f v_l^f + \frac{1}{2}(v_k^f + v_l^f) \right] - \bar{\chi}_{kl} \left[v_k^i v_l^i + \frac{1}{2}(v_k^i + v_l^i) \right] \right)
$$
(4)

where ΔE_{el} is the difference of energy between the minima of PES. Assuming that all transitions originate from the vibrational ground state of the initial electronic state, which is the case at very

low temperature, the previous equation can be recast as

$$\Delta\varepsilon_{if} = \Delta E_{00} + \sum_{k=1}^{N} v_k^f \overline{\overline{\omega}}_k + \sum_{k,l=1}^{N} \overline{\overline{\chi}}_{kl}\left[v_k^f v_l^f + \frac{1}{2}(v_k^f + v_l^f)\right]$$
(5)

with "$\Delta E_{00} = \Delta E_{el} + \overline{\overline{\varepsilon}}_0 - \overline{\varepsilon}_0$" the energy difference between the vibrational ground state of the two electronic states.

An alternative form of eq 5 can be derived using the VPT2 fundamental energies (ν_{1_k})

$$\Delta\varepsilon_{if} = \Delta E_{00} + \sum_{k=1}^{N} v_k^f \overline{\nu}_{1_k} + \sum_{k=1}^{N} \overline{\overline{\chi}}_{kk} v_k^f (v_k^f - 1) + \sum_{k \neq l}^{N} \overline{\overline{\chi}}_{kl} v_k^f v_l^f$$
(6)

3. COMPUTATIONAL DETAILS

All calculations were performed using the GAUSSIAN 16 suite of quantum chemical programs.[45] In this work, we used our implementation[5,21,23,42,46,47] of second-order vibrational perturbation theory (VPT2) which can provide an accurate description of both anharmonic vibrational energies and wave functions. Anharmonic frequencies and IR absorption intensities were calculated by numerically differentiating the analytical Hessian and electric dipole first derivatives, with a step of $\delta Q_i = 10$ pm amu$^{1/2}$ along each normal mode. The generalized VPT2 (GVPT2) model was used for the treatment of resonances. The identification of Fermi resonances was done through a two-step procedure based on the difference of energy between the resonant states and the deviation of the VPT2 term from a model variational system. Terms identified as resonant were removed from the VPT2 calculations and reintroduced subsequently through a variational treatment, together with Darling–Dennison resonances (see refs 21 and 42 for details).

Inclusion of anharmonic effects in vibronic calculations was done with an alternate version of eq 6, where the corrective terms based on the anharmonic χ matrix were ignored

$$\Delta\varepsilon_{if} = \Delta E_{00} + \sum_{k=1}^{N} v_k^f \overline{\nu}_{1_k}$$

In the past,[48,49] we employed a simplified method for the estimation of anharmonic effects for excited states based on those of the ground state. The method involved the use of the Duschinsky matrix, which relates the modes of the two states through the following equation:[50]

$$\overline{Q} = J\overline{\overline{Q}} + K$$
(7)

where $\overline{Q}$ and $\overline{\overline{Q}}$ are the normal modes of the initial and final electronic states, respectively, J is the Duschinsky matrix, and K is the shift vector. Once the anharmonic fundamental energies of the ground state ν are known, those of the excited state can be estimated, in the case of absorption spectra, as

$$\overline{\nu}_l = \left(\sum_k (J_{kl})^2 \frac{\overline{\nu}_k}{\overline{\omega}_k}\right)\overline{\overline{\omega}}_l$$
(8)

In some of the following examples, this method will be revisited in light of the new developments which allow the estimation of anharmonic effects through perturbation theory.

All vibronic simulations were performed using the time-independent framework via the sum-overstate method (see refs 30 and 31.).

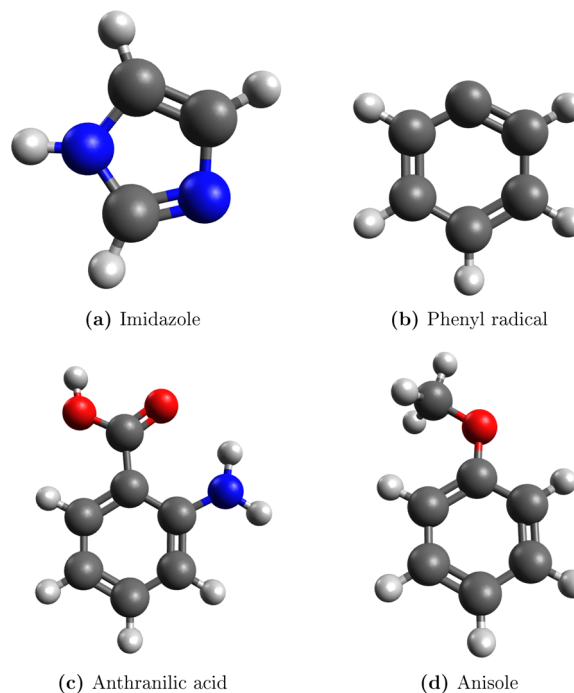All molecules studied in the work are shown in Figure 1.

(a) Imidazole

(b) Phenyl radical

(c) Anthranilic acid

(d) Anisole

Figure 1. Molecules studied in this work.

4. RESULTS AND DISCUSSION

4.1. Imidazole. We begin our discussion with imidazole, a simple model system that is ideal for illustrating characteristics of excited state vibrational spectra because of its small size and reliability of data regarding the spectroscopic properties of this molecule related to the vibrational degrees of freedom of the excited state.[49] All calculations on imidazole were performed using the B3LYP[51−53] functional and the aug-cc-pVTZ basis set.[54−56]

Like any numerical differentiation scheme, a possible source of error in the resulting anharmonic correction is a poor choice of the differentiation step, which should ideally be small but not so much that it leads to numerical errors due to the limited machine precision as well as the finite convergence criteria of the various steps in the calculation, such as the convergence on the SCF energy and density, the TDDFT transition energy and densities obtained through the Davidson algorithm,[57] the convergence criteria for the Coupled Perturbed Kohn–Sham (CPKS) and Coupled Perturbed TD-DFT equations, the finite accuracy of the DFT integration grid, and other numerical criteria. It might be tempting to simply employ the same differentiation step we have used in the past for ground-state calculations of 10 pm amu$^{1/2}$, which has been shown to yield reliable numerical derivatives. However, an excited-state PES is generally expected to be "flatter" than the ground state one; therefore, a different differentiation step might be preferable. To verify this assumption, we performed the anharmonic calculation on imidazole using multiple differentiation steps spanning different orders of magnitude to analyze the numerical stability of the results. Figure 2 displays the 1, 11, and 21 modes of imidazole, and Figure 3 reports the anharmonic energy and intensity for those modes. The first two
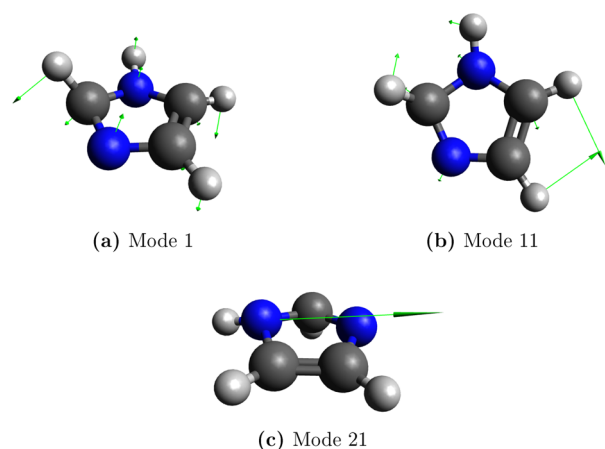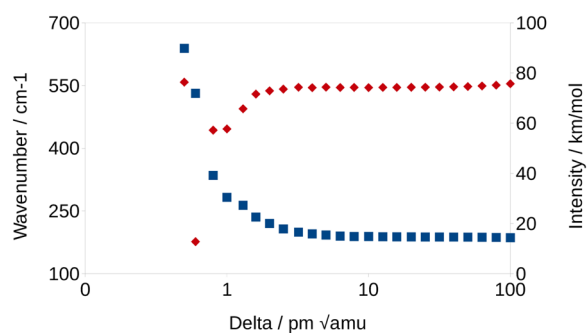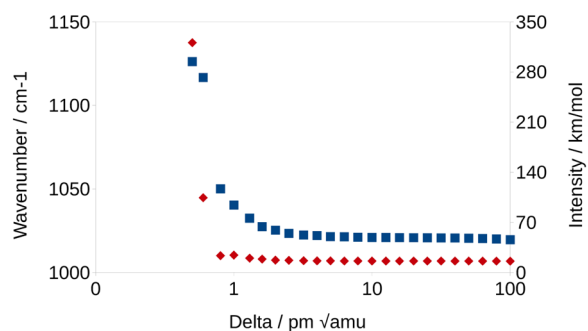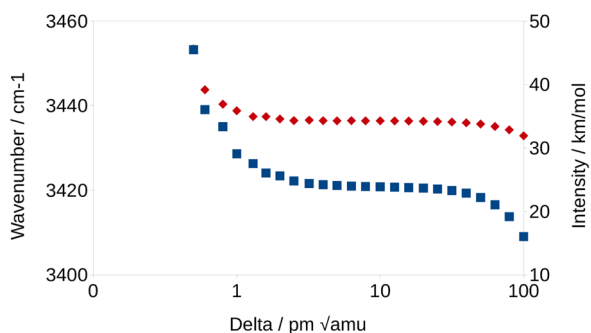
(a) Mode 1   (b) Mode 11

(c) Mode 21

Figure 2. Normal modes of imidazole in the excited state.

(a) Mode 1

(b) Mode 11

(c) Mode 21

Figure 3. Anharmonic energies (blue squares) and intensities (red diamonds) of imidazole calculated using different numerical differentiation steps for three representative normal modes.
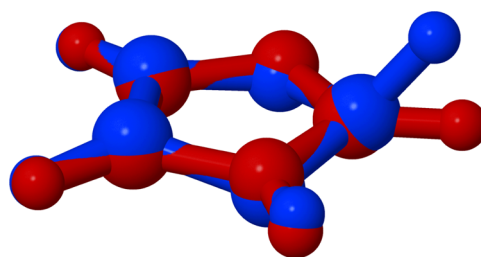

Figure 4. Structure of imidazole in the ground (red) and excited, S_1 electronic state (blue). The equilibrium structures have been computed at the B3LYP/aug-cc-pVTZ level of theory.
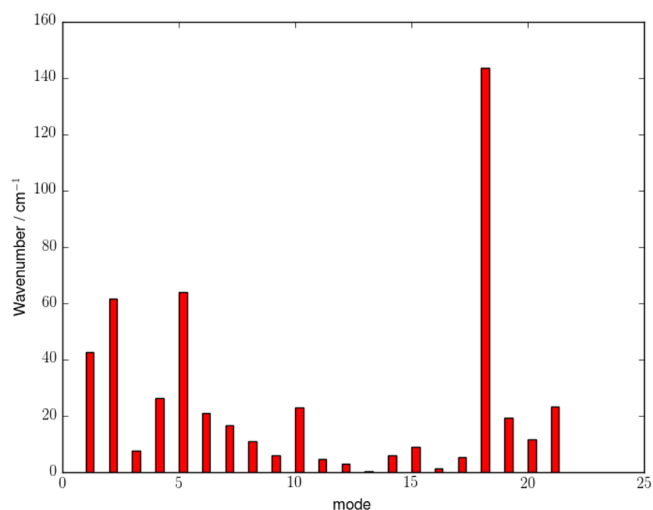

Figure 5. Absolute difference between the anharmonic frequencies of imidazole calculated using VPT2 and the Duschinsky-based method.
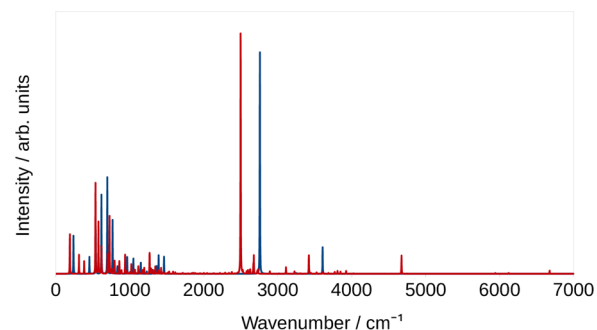

Figure 6. Harmonic (blue) and anharmonic (red) infrared spectra of imidazole in the excited state. Broadening effects have been included with Lorentzian broadening functions of 2 cm^{-1}.

modes are bendings involving most of the atoms in the ring, and the third is the NH stretching. Below a numerical value of 1 pm amu$^{1/2}$, the results become unstable for all three modes (more so for the lowest-energy one), while for the highest-energy mode instabilities in the numerical energy and intensity starts to appear at a value of 40. As shown in the figure, the ground-state default value of 10 generally lies at the middle of a plateau in the plots for both energies and intensities for all three modes, confirming the reliability of the chosen numerical differentiation step.

As mentioned in Section 3, in the past we employed a method based on the Duschinsky matrix to estimate anharmonic effects in the excited state. It was shown[49] that a significant discrepancy between the estimated and fully anharmonic results can be

Table 1. Harmonic, Anharmonic, and Extrapolated Frequencies for D_0 and D_1 states of Phenyl Radical Computed at B3LYP/SNSD level

Mode	Symm.	Harm. S_0	Anharm. S_0	Harm. S_1	Scal. S_1	Anharm. S_1
1	A_1	400.134	390.917	299.660	292.846	289.887
2	B_1	423.944	416.150	354.322	347.358	347.732
3	B_2	594.236	588.095	527.707	522.086	528.533
4	A_1	614.264	609.520	590.751	586.151	581.805
5	B_1	667.807	650.805	682.305	674.965	665.291
6	B_1	719.920	706.433	764.050	751.747	746.189
7	A_2	814.178	792.719	787.816	767.042	767.253
8	A_1	893.238	869.735	923.361	907.573	907.658
9	B_1	968.277	941.104	966.685	941.689	938.953
10	A_2	981.849	968.928	997.068	969.097	970.741
11	A_1	995.120	968.135	999.879	985.481	982.110
12	A_1	1014.756	999.397	1017.064	999.206	1001.350
13	B_1	1046.795	1025.039	1024.006	997.041	995.905
14	B_2	1068.810	1060.485	1048.727	1035.589	1040.082
15	B_2	1171.064	1157.918	1118.088	1103.633	1093.978
16	A_1	1171.845	1156.986	1213.744	1198.077	1193.132
17	B_2	1302.373	1277.038	1241.510	1222.394	1219.820
18	B_2	1334.222	1309.661	1349.836	1324.526	1320.665
19	B_2	1459.878	1431.567	1395.244	1368.014	1372.508
20	A_1	1467.893	1436.368	1442.357	1411.234	1411.309
21	B_2	1571.771	1529.905	1521.746	1490.773	1484.554
22	A_1	1629.513	1592.817	1632.013	1588.648	1578.686
23	A_1	3159.398	3016.322	3137.459	2998.836	3026.061
24	B_2	3165.760	3028.737	3137.860	3004.743	3003.548
25	A_1	3179.364	3040.669	3160.153	3020.954	3008.177
26	B_2	3181.599	3050.657	3165.820	3032.806	3029.222
27	A_1	3191.353	3077.070	3184.981	3068.758	3073.908
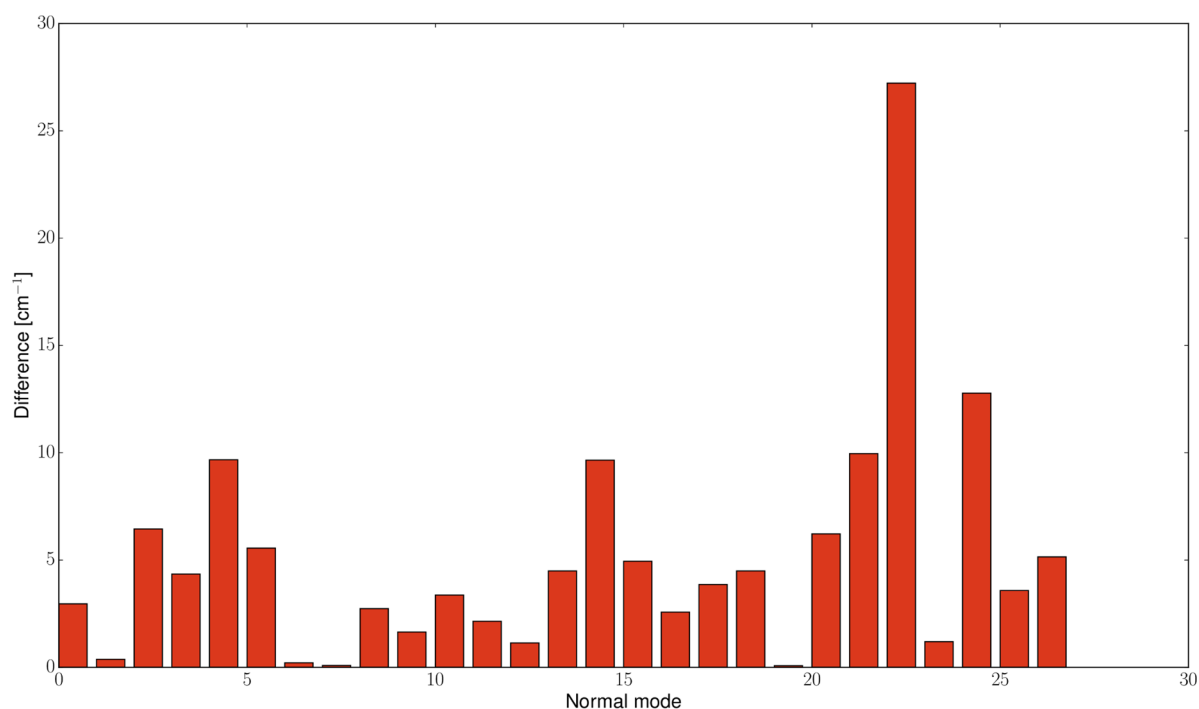
Figure 7. Plot of the absolute value of the difference between the anharmonic frequencies for the D_1 state of phenyl radical computed using the extrapolation based on the Duschinsky transformation and at the VPT2 level. Electronic structure calculations have been performed at the B3LYP/SNSD level.

observed when there is a large change in equilibrium geometry between the two states. This analysis was possible by focusing on states of different nature (such as the same molecule in an ionized form or in states of different spin multiplicity, which can be numerically treated as ground states). Here, we extend the analysis to the bright singlet $\pi-\pi^*$ transition. The equilibrium
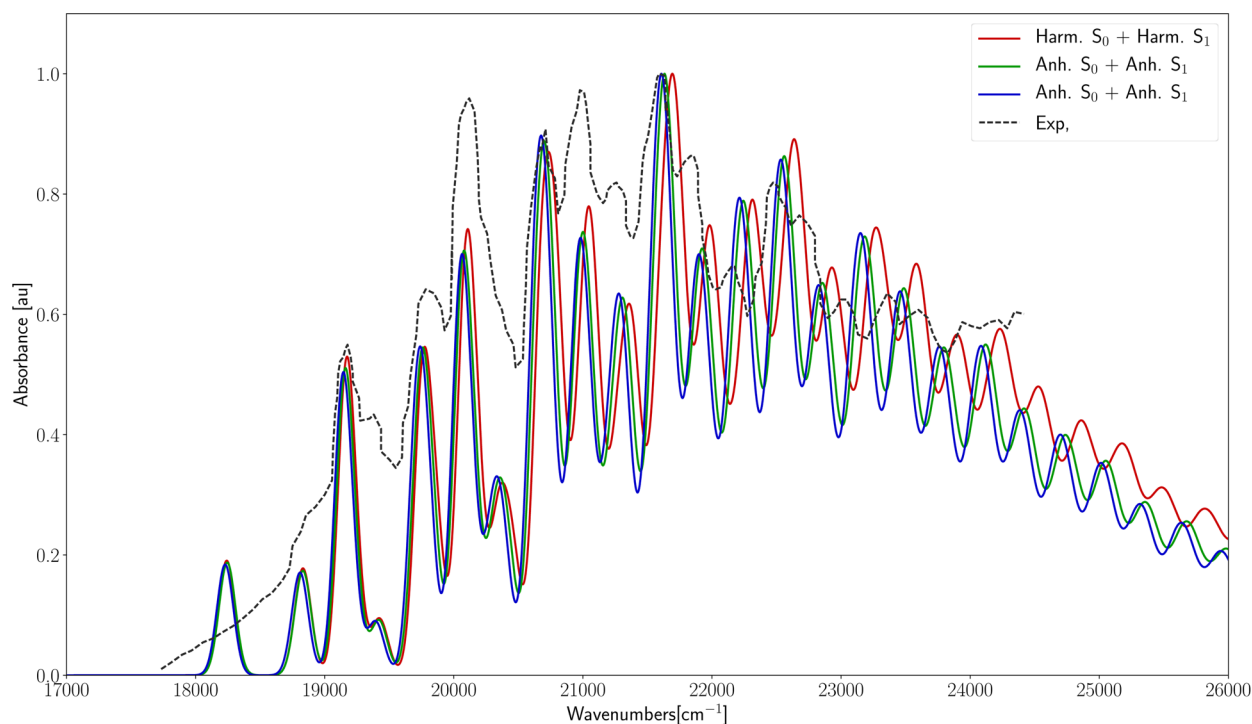
Figure 8. Theoretical OPA spectrum for the $D_1 \leftarrow D_0$ transition of phenyl radical, computed at the AH|FC level using the harmonic frequencies for both the electronic states (solid, red line), the anharmonic frequency for the S_0 state and the extrapolated ones for the S_1 state (solid, green line), and the anharmonic frequencies for both states (solid, blue line). The experimental spectrum is also shown (dashed, black line).[61] Broadening effects have been included with Gaussian broadening functions of 75 cm^{-1}.
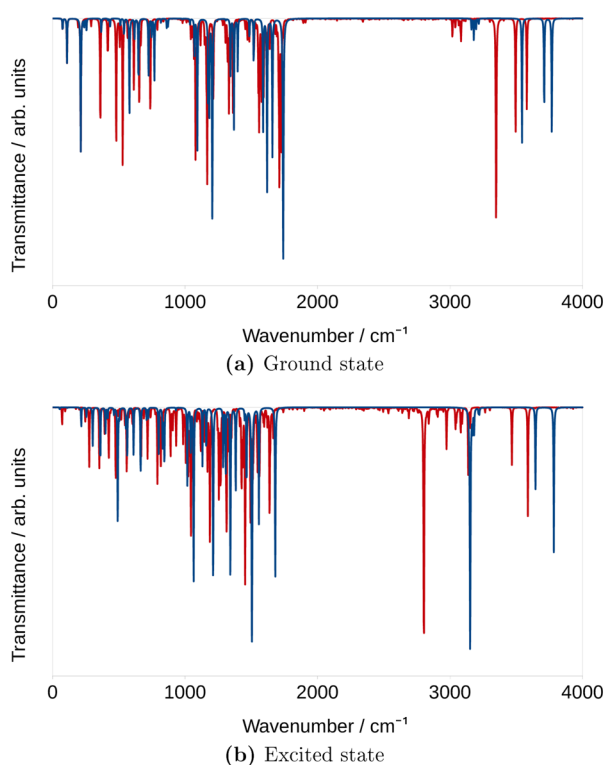

Figure 9. Harmonic (blue) and anharmonic (red) infrared spectra of antranilic acid. Broadening effects have been included with Lorentzian broadening functions of 2 cm^{-1}.

excited-state geometry for this system is also significantly distorted with respect to the ground-state one, as displayed in Figure 4. In Figure 5, the absolute difference between the

anharmonic frequencies of imidazole calculated using VPT2 and Duschinsky-based method is plotted for each mode. The first few modes are internal ring bendings, but the mode that shows the greatest deviation is, unsurprisingly, mode 18 which is the C−H stretching motion of the carbon that sits between the nitrogen atoms and is the one that undergoes pyramidalization in the excited state. The force field for that hydrogen atom is most affected by the pyramidalization; thus, it is poorly described in terms of contributions obtained from the ground state.

In addition to the energies, with the second and third derivatives of the excited-state dipole, it is possible to calculate the excited-state anharmonic infrared spectrum, including both electrical and mechanical anharmonicities. The harmonic and anharmonic spectra obtained this way are compared in Figure 6. The difference between the two spectra is significant. In addition to the expected redshift and the change in intensity of the harmonic bands, numerous overtone and combination bands enrich the spectrum. Unfortunately, to the best of our knowledge, an experimental spectrum of excited gaseous imidazole is not available for comparison.

4.2. Phenyl Radical. The next test case studied in the present work is the phenyl radical. Spectroscopic techniques (usually time resolved) are routinely used for the characterization of radicals, and for the phenyl radical, the high-resolution infrared[58,59] and electronic[60,61] spectra are available in the literature. In particular, the importance of vibronic effects on the electronic spectrum has been investigated by Kim and co-workers[62] and later by some of us[63,64] using more refined models, using anharmonic frequencies for the D_1 state computed through the extrapolation based on the Duschinsky transformation. Following the same analysis as for the previous system, the reliability of this approximation will be checked by computing the anharmonic frequencies of the excited, D_1 state at the VPT2 level.
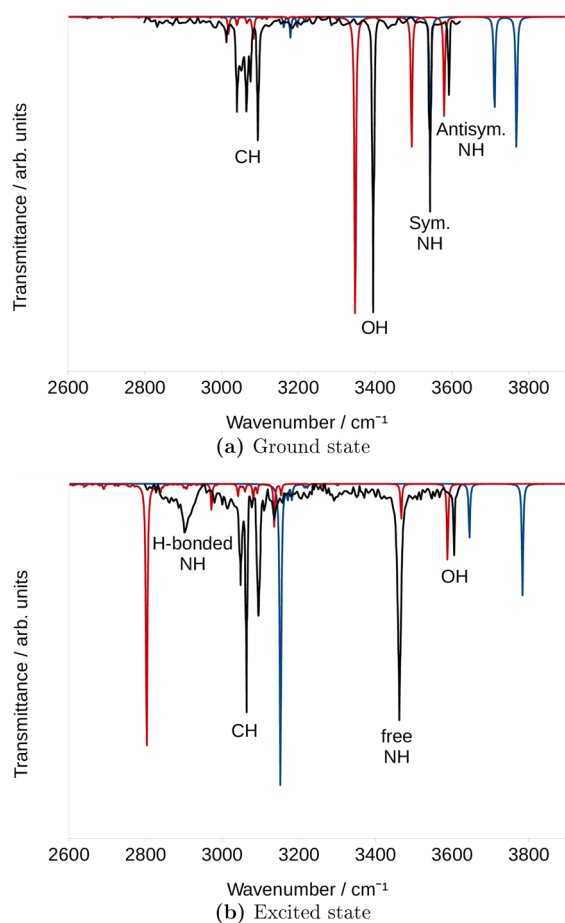
(a) Ground state

(b) Excited state

Figure 10. Comparison between the calculated harmonic (blue), anharmonic (red), and experimental[65] (black) ground and excited state infrared spectra of anthranilic acid. Assignment information refers to the experimental peaks. Broadening effects have been included with Lorentzian broadening functions of 2 cm^{-1}.

The harmonic and anharmonic frequencies for the D_0 and D_1 electronic states of phenyl, computed at the B3LYP/SNSD level, are reported in Table 1. This comparison shows that, in this case, the extrapolation scheme based on the Duschinsky transformation is significantly more reliable than for imidazole and anisole (*vide infra*) since, for the majority of the modes, the deviation between the extrapolated and VPT2 anharmonic frequencies is below 10 cm^{-1}. As shown in Figure 7, a graphical representation of the deviation between the two sets of frequencies, the largest difference is present for the higher-energy frequencies, above 3000 cm^{-1}, corresponding to the C–H stretching modes. Those modes are usually affected by strong anharmonic couplings, and therefore, the extrapolation scheme, which assumes that the anharmonic correction to the PES is the same for both the electronic states, is inaccurate. On the other hand, for the other modes, the accuracy is better due to the limited mode-mixing associated with the electronic transition.

The vibronic UV-absorption spectrum for the $D_1 \leftarrow D_0$ transition of the phenyl radical computed using three different sets of frequencies—harmonic for both states, anharmonic (VPT2) for both states, and anharmonic (VPT2) for the D_0 state and anharmonic (extrapolated) for the D_1 one—is reported in Figure 8. As already noticed before, the spectrum computed at the harmonic level is shifted toward higher energies with respect to the two anharmonic ones, which are nearly superimposable. As discussed in our previous work,[63] the main vibronic

Table 2. Comparison of Theoretical Frequencies, Computed at Harmonic and Anharmonic Levels, of S_0 Electronic State of Anisole with Experimental Data, Taken from Ref 78[a]

Mode	Harm.	Anharm.	HRAO
1	90.43	83.05	92.56
2	204.10	128.53	192.67
3	255.86	252.02	254.90
4	267.52	326.13	241.57
5	421.90	416.25	416.26
6	445.94	437.48	441.08
7	517.18	508.79	510.84
8	560.35	553.80	553.00
9	629.06	623.21	622.98
10	696.94	694.19	693.58
11	763.71	761.68	762.01
12	797.18	783.97	783.50
13	827.41	811.83	812.00
14	893.78	883.08	882.03
15	971.16	958.03	957.91
16	989.48	980.56	980.66
17	1009.26	994.05	994.35
18	1040.58	1024.13	1018.33
19	1065.01	1041.73	1041.20
20	1102.25	1082.63	1082.63
21	1169.31	1146.96	1144.84
22	1178.28	1164.19	1164.26
23	1194.35	1180.15	1179.14
24	1201.47	1178.01	1177.50
25	1271.41	1238.54	1238.48
26	1334.51	1303.56	1303.42
27	1356.98	1338.77	1339.16
28	1473.86	1440.00	1435.84
29	1484.96	1451.00	1450.62
30	1493.10	1454.16	1450.34
31	1505.53	1470.40	1470.69
32	1526.54	1497.62	1498.45
33	1624.19	1582.63	1582.76
34	1641.96	1601.25	1601.55
35	3002.56	2819.80	2812.86
36	3060.48	2894.14	2888.20
37	3131.99	2993.66	2991.28
38	3163.07	3005.47	3005.64
39	3170.49	3035.63	3035.83
40	3186.65	3044.40	3043.40
41	3193.97	3073.76	3074.75
42	3204.08	3087.85	3087.99

[a]Electronic structure calculations have been performed at the B3LYP/6-311+G(d,p) level.

progressions of the vibronic spectrum of phenyl correspond to excitation of two modes (4 and 8) with low-frequency (below 1000 cm^{-1}), and in this region, the extrapolation scheme is reliable. Figure 8 also reports the experimental spectrum, shifted by 873 cm^{-1} to more closely match the calculated ones at the position of the first peak. The inclusion of anharmonicity effects, using either scheme, generally improves the agreement with the experiment for the higher-energy peaks in the vibronic progression, for which the anharmonic shifts add up to noticeable values.

4.3. Anthranilic Acid. We applied our method to the calculation of the excited-state infrared spectrum of anthranilic acid (Figure 1c), a molecule chosen because of its limited size,

Table 3. Comparison of Theoretical Frequencies, Computed at Harmonic and Anharmonic Levels, of S₁ Electronic State of Anisole with Experimental Data, Taken from Ref 73[a]

Mode	Harm.	Anharm.	Scal.	RD-HRAO	Exp.[73]
1	63.05	272.66	61.15	62.95	66
2	78.41	84.36	74.11	86.76	85
3	135.76	90.19	103.59	151.79	140
4	196.89	214.57	210.66	193.91	197
5	253.58	232.57	249.76	248.92	256
6	374.48	368.27	370.57	383.23	372
7	436.26	429.32	428.05	431.20	421
8	439.95	501.03	433.04	472.27	436
9	517.18	500.15	511.86	505.59	509
10	527.70	514.24	522.45	513.39	524
11	546.03	539.85	540.06	537.23	538
12	600.76	639.13	592.84	607.36	595
13	625.72	625.95	622.66	620.75	620
14	678.51	732.90	671.15	706.93	670
15	780.78	765.32	767.82	765.47	772
16	856.76	848.28	848.53	839.50	845
17	973.59	952.92	958.66	956.29	960
18	989.52	969.66	972.93	970.60	972
19	1005.95	979.69	986.82	985.90	982
20	1034.30	1017.35	1013.94	1006.83	1008
21	1143.46	1120.22	1121.53	1115.68	1118
22	1151.93	1126.95	1136.58	1127.34	1127
23	1159.64	1140.87	1144.56	1141.35	1135
24	1183.19	1151.11	1161.45	1159.95	1161
25	1278.16	1236.68	1246.91	1236.95	1258
26	1309.62	1281.06	1282.96	1282.82	1277
27	1395.35	1359.16	1370.24	1359.78	1364
28	1419.44	1381.56	1386.67	1385.03	1389
29	1447.79	1400.48	1415.95	1402.13	1417
30	1457.23	1423.70	1423.11	1413.14	1424
31	1475.82	1437.98	1445.91	1441.32	1446
32	1482.91	1443.78	1444.21	1437.54	1443
33	1494.87	1448.56	1460.11	1452.44	1454
34	1521.22	1460.07	1483.56	1470.30	1482
35	3030.33	2935.65	2846.15	2933.33	2928
36	3099.48	2959.25	2931.04	2947.07	2980
37	3152.67	3008.49	3013.30	3006.01	3025
38	3170.29	3023.41	3022.15	3031.52	3042
39	3199.72	3088.89	3063.79	3050.99	3066
40	3207.43	3018.43	3058.30	3046.15	3078
41	3222.05	3122.60	3098.07	3102.47	3117
42	3228.20	3005.11	3109.82	3079.25	3128

[a]Electronic structure calculations have been performed at the B3LYP/6-311+G(d,p) level.

structural rigidity, and because of the availability of experimental data[65] as well as theoretical simulations[66] with which to compare our computational results. For this system, we chose the B3LYP functional,[51−53] the same employed in a previous study,[66] and the SNSD basis set.[67] In particular, we consider the first singlet excited state (S₁), hence, a π−π* transition. In the ground state, the amino group is slightly pyramidalized, whereas in the excited state the geometry is perfectly planar. Though in a previous work[66] the vibrational properties of the ground state were evaluated after imposing a constraint on the molecule to preserve the planarity, since our approach is rooted in perturbation theory, it is imperative that the reference state be a true minimum; therefore, we relaxed the symmetry constraint. The spectra are shown in Figure 9. For both ground and excited states, inclusion

of anharmonic effects causes the bands to be redshifted, especially those in the X-H stretching region (where X is a heavy atom). Regarding the intensities, an interesting feature of the anharmonic spectra is the change in the relative intensities between the X-H stretchings and the bendings. In the harmonic spectra, the two sets of bands have similar intensities, whereas the in the anharmonic spectra the latter are somewhat quenched, though this effect is not uniform and does not apply to every band; thus, the inclusion of anharmonic effects on both energies and intensities can be crucial for the analysis of the spectrum. In Figure 10, we compare the calculated and experimental[65] spectra for both ground and excited states, limited to the X-H stretching region. In the ground-state spectra, we can observe the expected and significant redshift of all bands as anharmonicity effects are considered. The anharmonic bands are much closer to the experimental ones, though the anharmonic correction tends to be too large in some cases. Intensities are also greatly improved by the perturbative correction. In particular, the relative intensity of the symmetric and antisymmetric N−H stretchings is incorrect in the harmonic spectrum, where the latter has a larger relative intensity, contrary to what can be observed in both experimental and anharmonic spectra. The intensities of the aromatic C−H stretching bands, however, are much higher in the experimental spectrum compared to the calculated one, and anharmonic effects do not significantly increase intensities for these peaks. In the excited-state spectrum the agreement between theory and experiment is significantly worse. The relative intensity of the O−H stretching and free N−H stretching bands is not inverted by including anharmonic effects (though the frequencies still show excellent agreement). As in the ground-state spectrum, the intensity of the aromatic C−H stretching bands is much lower in the computed spectrum compared to the experimental one. Furthermore, while theory successfully predicts a very strong redshift in the H-bonded N−H stretching band, which is accompanied by a very large anharmonic shift, the intensity of this band is very low in the experimental spectrum, while it is very high in the calculated one. These results show that there is a need for extensive computational benchmarks for excited-state properties in order to identify the best DFT functional and basis set requirements to perform these types of calculations. This type of study would require a wide set of experimental data, possibly together with accurate calculations performed using higher levels of theory, and is beyond the scope of this work.

4.4. Anisole. The third test-case system studied in this work is anisole (which is the methyl ester of phenol, the structure is reported in Figure 1d). The spectroscopic properties of anisole in gas phase have been characterized using a wide range of experimental techniques, ranging from rotational[68] to vibrational[69,70] and electronic spectroscopies.[71−73] More recently, dimers[74] and van der Waals complexes of anisole have also been characterized spectroscopically.[75−77] From a theoretical point of view, the high-resolution vibronic spectrum of free anisole has been simulated by some of us[78] using the Adiabatic Hessian Franck−Condon model (AH|FC model, see refs 79 and 80 for details) and the anharmonic frequencies of the excited electronic state (S₁) estimated using the extrapolation scheme introduced in Section 2. As discussed in ref 78, this extrapolation scheme provides a systematic improvement of the theoretical one-photon absorption (OPA) spectrum compared to the experimental one.[73] Here, the reliability of the extrapolation will be further tested by comparing those frequencies to the anharmonic ones, computed at the GVPT2 level.
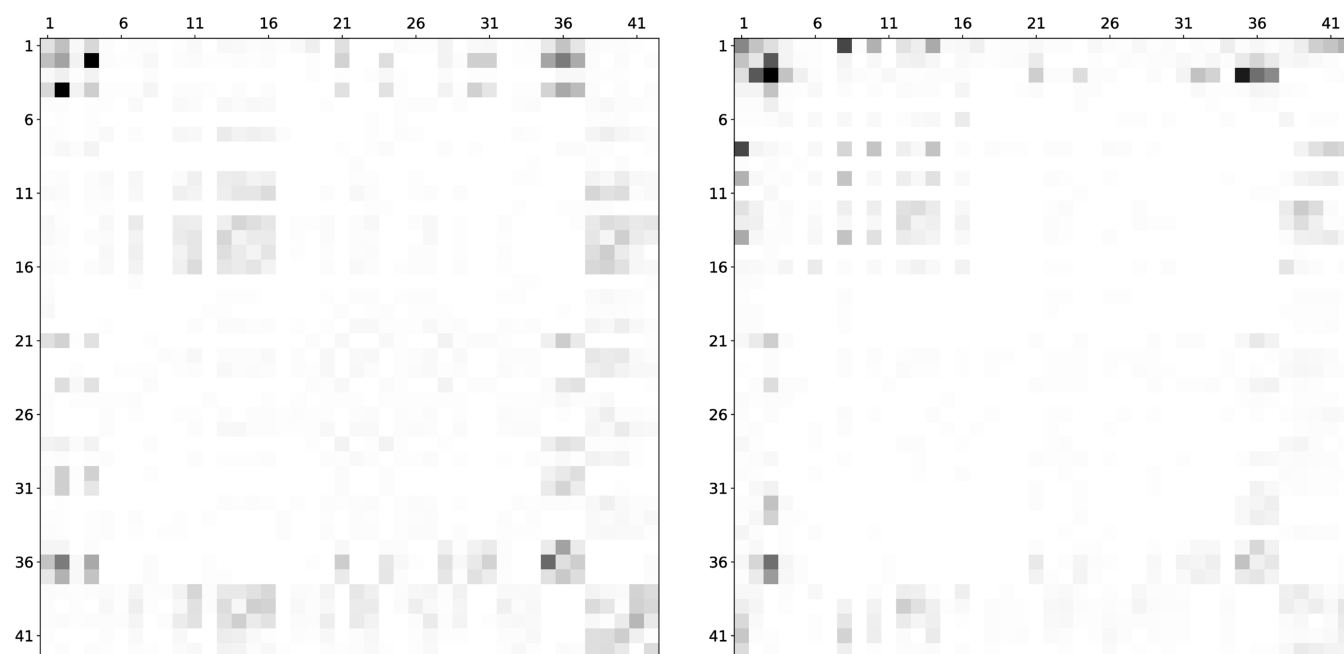
Figure 11. Graphical representation of the anharmonic Υ matrix of anisole in the S_0 (left panel) and S_1 (right panel) states. The representation has been obtained as follows: Elements Υ_{ij}^2 are calculated and normalized to 1. Then, a shade of gray is associated with each element (i,j) in the figure based on the equivalence (0, white; 1, black). The normalization factor is 284.31 cm^{-1} for the S_0 state and 648.64 cm^{-1} for the S_1 state.
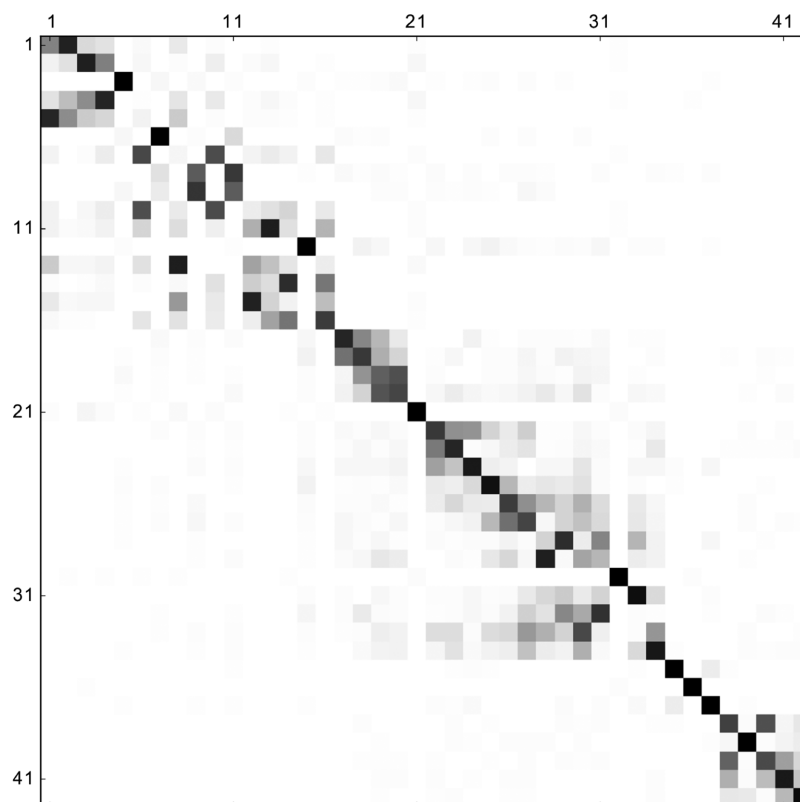

Figure 12. Graphical representation of the Duschinsky matrix **J** for the $S_1 \leftarrow S_0$ transition of anisole. The representation is obtained as already discussed for Figure 11.

The harmonic and anharmonic frequencies of the ground and excited electronic states are reported in Tables 2 and 3, together with the experimental frequencies of the S_1 state, taken from ref 78. For the sake of consistency with our previous work,[78] electronic structure calculations have been performed at the B3LYP/6-311+G(d,p) level. For the ground electronic state,

a full, direct GVPT2 treatment leads to an overall lowering of most of the frequencies, with the exception of the fourth mode that displays an anharmonic correction of +59 cm^{-1}. As emerges from an hindered rotor analysis,[81] this mode, together with the lowest-energy one (with harmonic frequency of $\omega_1 = 90.43$ cm^{-1}), corresponds to torsions about the two single C−O bonds of
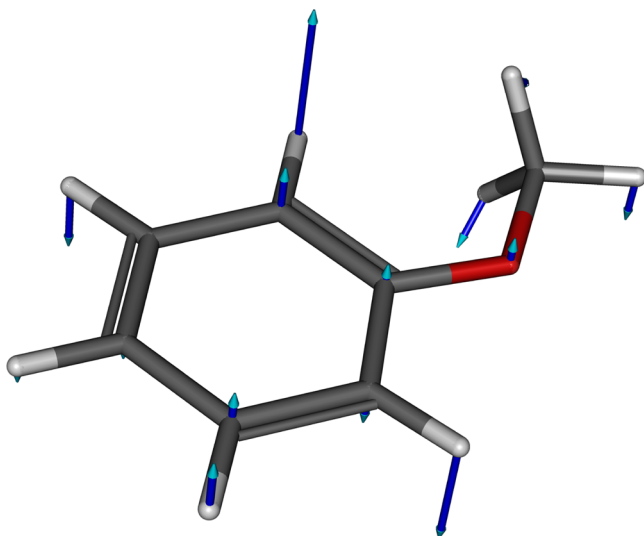
Figure 13. Graphical representation of the lowest-energy harmonic mode of the S_1 state of anisole computed at the B3LYP/6-311+G(d,p).

the molecule. Such large-amplitude modes (LAMs) are highly anharmonic and thus poorly described at a perturbative level based on a quartic force field. In order to get more reliable results, all the couplings between the LAMs and the other modes have been canceled,[82] and LAMs have been treated using the hindered rotor model (the combined model is referred to as Hindered Rotor Anharmonic Oscillator, HRAO).[83] As shown in Table 2, for most of the modes, the difference between the full dimensionality and the HRAO results is below 2 cm^{-1}, with the exception of modes 18, 28, 35, and 36. Therefore, the couplings between the two LAMs and the other modes is not critical, and thus, the HRAO model, where those couplings are neglected, is a satisfactory approach.

To further evaluate the extent of the coupling between the modes, a graphical representation of the anharmonic Υ matrix (defined in the Appendix) is reported in the left panel of Figure 11. As expected, most of the couplings between the LAMs (modes 1 and 4) and the other modes are nearly null, with the exception of modes 35 and 36 (which are in fact among the ones displaying the largest deviation between the full-dimensional and the HRAO schemes).

For the excited, S_1 state, modes 2 and 3 are the ones corresponding to the torsions along the two C—O single bonds, as confirmed by the graphical representation of the Duschinsky matrix $\mathbf{J}$, reported in Figure 12. In this case as well, the Υ matrix (right panel, Figure 11) shows a coupling of those modes mainly with mode 36. However, in addition to the two internal rotations, an additional, low-frequency mode (with harmonic wavenumber $\omega_1 = 63.05$ cm^{-1}) is present. The plot of the Duschinsky transformation shows that this mode corresponds to mode 5 of the ground state, with harmonic wavenumber of 421 cm^{-1}. As shown in Figure 13, this mode is an out-of-plane deformation of the ring, and the lowering of its frequency is probably due to the transfer of electron density to π^* orbitals of the aromatic ring upon electronic excitation, which makes the ring less stable. The anharmonic frequencies of the S_1 electronic state of anisole computed at the VPT2 level, that are collected in Table 3, show that full-dimensional VPT2 calculations lead to an unphysical anharmonic correction for the first mode (anharmonic frequency is approximately 3 times larger than its harmonic counterpart). To obtain more reliable results, the force constants involving the first mode have been neglected, and this mode has been treated at the harmonic level.[82] Furthermore, the two torsional modes have been treated at the HRAO level, and the results (labeled as reduced-dimensionality HRAO, RD-HRAO) are collected in Table 3, together with the results obtained using the extrapolation based on the Duschinsky transformation $\mathbf{J}$. At variance with the ground electronic state, in this case, the difference between the full-dimensional and the RD-HRAO models is more significant, above 2 cm^{-1} for the majority of the modes.
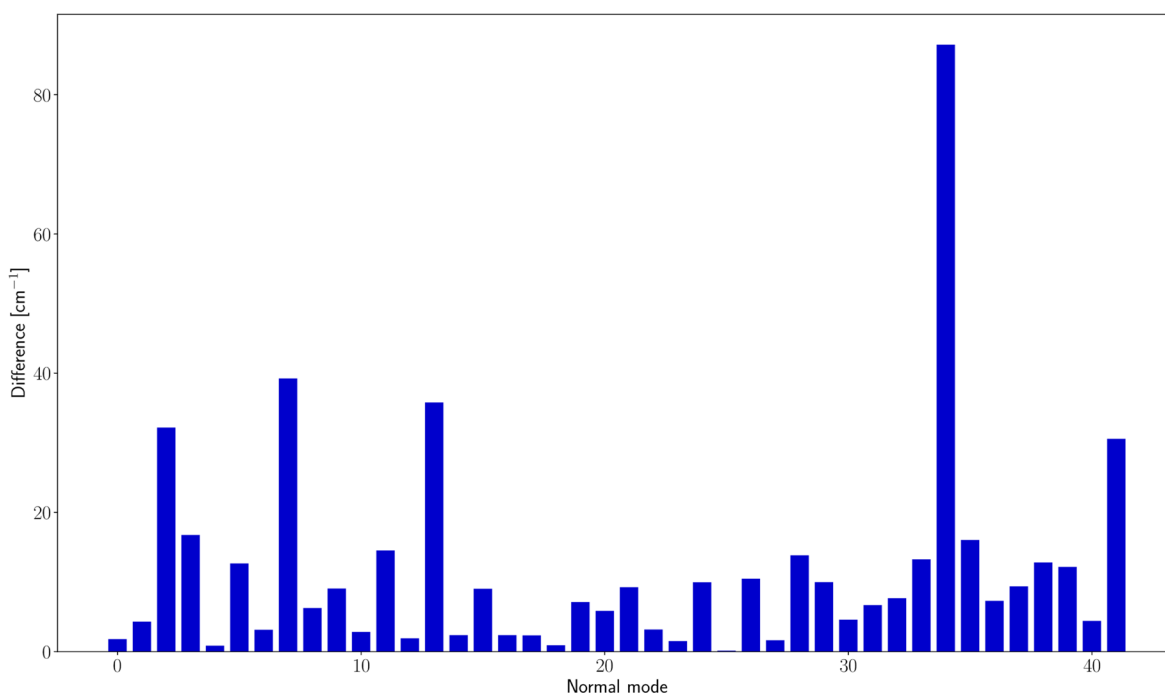

Figure 14. Graphical representation of the difference between the anharmonic frequencies computed at the VPT2 level and the ones determined using the extrapolation based on the Duschinsky transformation.
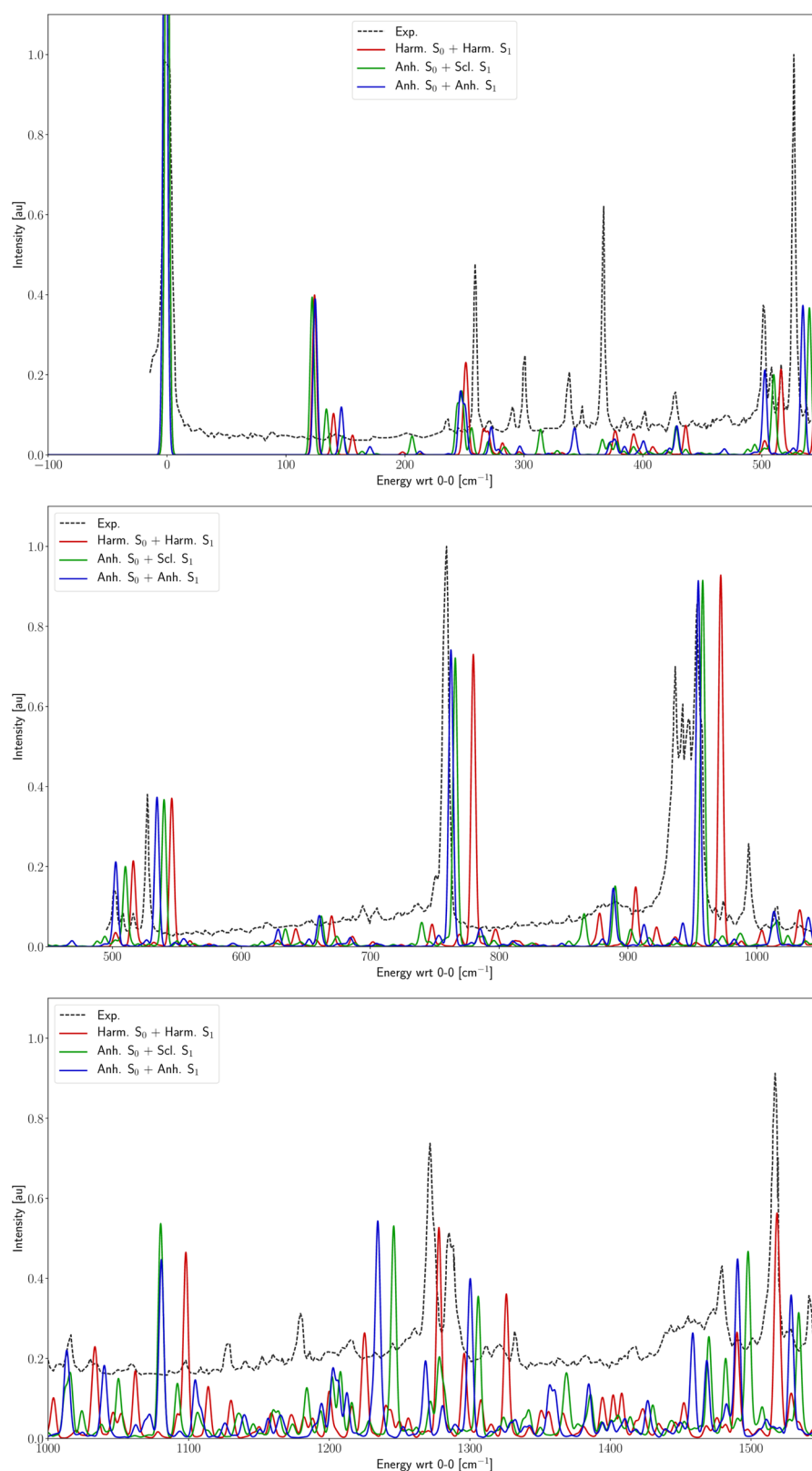
Figure 15. Comparison of the theoretical (TI AH|FC level) and experimental[73] $S_1 \leftarrow S_0$ OPA spectrum of anisole. Theoretical spectra have been computed using the harmonic frequencies for both the electronic states (solid red line), the anharmonic frequencies for the S_0 state, and the extrapolated ones for the S_1 state (solid, green line) and the anharmonic frequencies for both the states (solid, blue line). Gaussian functions with an HWHM of 2 cm^{-1} have been used to reproduce broadening effects.

This means, in practice, that the coupling between the LAMs and the other modes is larger than for the ground state, and therefore, the difference between the reduced- and the full-dimensional

systems is higher. This result reveals that there is a significant change in the anharmonic component of the PES between the two electronic states, and in this case, the extrapolation technique

based on the Duschinsky transformation is expected to work poorly. In fact, as shown in Figure 14, the difference between the anharmonic frequencies computed using the two approaches is significant, above 20 cm^{-1} for several modes. It is noteworthy that the difference is large not only for the low-frequency modes but also for the higher-energy ones, with the largest deviation occurring for mode 34. This further confirms that anharmonic effects are significantly different for the two electronic states, and the extrapolation technique is, in this case, inaccurate.

Finally, the anharmonic frequencies computed using both approaches have been used to simulate the OPA spectrum of anisole at the AH|FC level, following the procedure discussed in Section 3. The results of the simulation are reported in Figure 15 and compared with the experiment from ref 73. Inclusion of anharmonic effects for the S$_1$ state, either using the extrapolation approach or the VPT2 one, leads to an overall redshift of the bands, with this shift being larger for the VPT2 frequencies than for the extrapolated ones. This trend can be observed, for example, in the region between 800 and 1500 cm^{-1} (with respect to the 0−0 transition) of the spectrum, which is reported in the middle panel of Figure 15 and is characterized by three intense bands (at about 550, 750, and 950 cm^{-1}, respectively). The position of those is overestimated at the harmonic level, and this inaccuracy is only partially corrected using the extrapolated anharmonic frequencies. Frequencies computed at the VPT2 level for both S$_0$ and S$_1$ electronic states provide even better band positions, resulting in an overall improvement in the quality of the spectrum. A similar trend is detected also for other regions of the spectrum, even if in this case the agreement can be less satisfactory, especially in the 0−500 cm^{-1} range. However, this energy range contains large-amplitude motions, which could not be treated at a satisfactory level of theory in the present study.

5. CONCLUSIONS AND PERSPECTIVES

In this paper, we have presented calculations of anharmonic frequencies and infrared (IR) absorption intensities for molecular systems in excited electronic states computed by means of vibrational perturbation theory, as well as vibronically resolved absorption spectra computed using the anharmonic frequencies to model both ground and excited state potential energy surfaces. These developments have been made possible thanks to the availability of analytical TDDFT second derivatives,[24−28] from which numerical third and semi-diagonal fourth derivatives can be evaluated, in addition to the second and third derivatives of the molecular dipole moments which are responsible for the so-called electrical anharmonicity of IR absorption spectra. In addition, anharmonic corrections were also employed to obtain a more accurate vibronic band shape for one-photon absorption spectra.

The results show that the numerical differentiation scheme commonly adopted for ground-state calculations can be carried over to excited states without change. The treatment of vibrational resonances, such as Fermi and Darling−Dennison resonances, can also be applied in the same way, ensuring the stability of the computed frequencies. The VPT2 strategy can replace earlier methods for estimating excited-state anharmonic frequencies, such as the Duschinsky-based method or simple scaling methods. Having a solid theoretical foundation, the applicability of the method is large, with the computational cost of the numerical derivatives being the limiting factor, though the latter can be run in parallel, reducing the time needed to obtain the anharmonic force field.

There is still much work to be done in this field. The extension of the current methodology to other types of vibrational spectroscopies, such as vibrational circular dichroism (VCD) or Raman scattering, is subject to the availability of analytical excited-state properties and their derivatives (such as derivatives of the electronic polarizability for Raman), so that their numerical anharmonic derivatives may be computed. In addition, the present study only considered isolated molecules, though in the case of molecules in the ground state much work has been done to include environmental effects in the calculation, particularly in the case of solvation. Analytical TDDFT derivatives have been presented for molecules coupled with both a polarizable continuum[84] and an atomistic classical environment.[85] However, one difficulty is the correct identification of the solvation regime that should be employed for such calculations, especially in the case of continuum models, for which different solvation regimes have been shown to drastically alter spectroscopic responses, particularly when both electronic and vibrational excitations are involved.[49] A further improvement of the model would be possible employing curvilinear internal coordinates in the description of molecular vibrations. It has been shown that, for vibronic spectroscopy, the use of internal coordinates leads to a different, more diagonal definition of the Duschinsky transformation.[86,87] As a consequence, this would increase the reliability of the extrapolation scheme discussed in the present work. However, the use of this scheme would require the calculation of anharmonic frequencies of the ground state at the VPT2 level, which is far from being trivial, even if some pilot works have been proposed recently in this direction.[88,89]

■ APPENDIX

Mode Coupling Analysis in VPT2 Calculations

The most compact notation for VPT2 vibrational energies (see eq 3) uses a single matrix, at least for asymmetric tops, which represents the anharmonic corrections, noted here as χ:

$$16\chi_{ii} = k_{iiii} - \frac{5k_{iii}^2}{3\omega_i} - \sum_{\substack{j=1 \\ j \neq i}}^{N} \frac{(8\omega_i^2 - 3\omega_j^2)k_{iij}^2}{\omega_j(4\omega_i^2 - \omega_j^2)} \tag{9}$$

$$4\chi_{ij} = k_{iijj} - \frac{2\omega_i k_{iij}^2}{(4\omega_i^2 - \omega_j^2)} - \frac{2\omega_j k_{ijj}^2}{(4\omega_j^2 - \omega_i^2)} - \frac{k_{iii}k_{ijj}}{\omega_i} - \frac{k_{jjj}k_{iij}}{\omega_j}$$
$$+ \sum_{\substack{k=1 \\ k \neq i,j}}^{N} \left[\frac{2\omega_k(\omega_i^2 + \omega_j^2 - \omega_k^2)k_{ijk}^2}{\Delta_{ijk}} - \frac{k_{iik}k_{jjk}}{\omega_k} \right]$$
$$+ \frac{4(\omega_i^2 + \omega_j^2)}{\omega_i\omega_j} \sum_{\tau=x,y,z} B_\tau^{eq}\{\zeta_{ij,\tau}\}^2 \tag{10}$$

with $\Delta_{ijk} = \omega_i^4 + \omega_j^4 + \omega_k^4 - 2(\omega_i^2\omega_j^2 + \omega_i^2\omega_k^2 + \omega_j^2\omega_k^2)$

While convenient for implementations, this form is not suitable to analyze the contributions of a single mode or the coupling between two modes to the energy of a given state. A simple solution is to split χ in two matrices, Υ and Z, defined as follows:

$$16\Upsilon_{ii} = k_{iiii} - \frac{5k_{iii}^2}{3\omega_i} \tag{11}$$

$$4\Upsilon_{ij} = k_{iijj} - \frac{[2\omega_i + (8\omega_i^2 - 3\omega_j^2)]k_{iij}^2}{(4\omega_i^2 - \omega_j^2)} - \frac{2\omega_j k_{ijj}^2}{(4\omega_j^2 - \omega_i^2)}$$

$$- \frac{k_{iii}k_{ijj}}{\omega_i} - \frac{k_{jjj}k_{iij}}{\omega_j} + \frac{4(\omega_i^2 + \omega_j^2)}{\omega_i\omega_j} \sum_{\tau=x,y,z} B_\tau^{eq} \{\zeta_{ij,\tau}\}^2 \tag{12}$$

$$4Z_{ijk} = (1 - \delta_{ik})(1 - \delta_{jk})\left[\frac{2\omega_k(\omega_i^2 + \omega_j^2 - \omega_k^2)k_{ijk}^2}{\Delta_{ijk}} - \frac{k_{iik}k_{jjk}}{\omega_k}\right] \tag{13}$$

With those matrices, the vibrational energy becomes

$$\varepsilon_m = \varepsilon_0 + \sum_{i=1}^N v_i^m \omega_i + \sum_{i,j=1}^N \left(\Upsilon_{ij} + \sum_{k=1}^N Z_{ijk}\right)\left[v_i^m v_j^m + \frac{1}{2}(v_i^m + v_j^m)\right] \tag{14}$$

■ ASSOCIATED CONTENT

Ⓢ Supporting Information

The Supporting Information is available free of charge on the ACS Publications website at DOI: 10.1021/acs.jctc.7b00218.

> Ground and excited state geometries for all molecules presented in this work (PDF)
> Movie of normal Mode 1 depicted in Figure 2. (AVI)
> Movie of normal Mode 11 depicted in Figure 2. (AVI)
> Movie of normal Mode 21 depicted in Figure 2. (AVI)
> Movie of normal mode depicted in Figure 13. (AVI)

■ AUTHOR INFORMATION

Corresponding Authors

*E-mail: xsli@uw.edu (X.L.).
*E-mail: vincenzo.barone@sns.it (V.B.).

ORCID ⓘ

Franco Egidi: 0000-0003-3259-8863
Alberto Baiardi: 0000-0001-9112-8664
Xiaosong Li: 0000-0001-7341-6240

Author Contributions

⊥F. Egidi, D. B. Williams-Young, and A. Baiardi contributed equally to this work.

Notes

The authors declare no competing financial interest.

■ REFERENCES

(1) Jensen, P.; Bunker, P. R. *Computational Molecular Spectroscopy*; Wiley, Chichester, U.K., 2000.

(2) Barone, V. *Computational Strategies for Spectroscopy: From Small Molecules to Nano Systems*; Wiley, Hoboken, NJ, 2011.

(3) Christiansen, O. Vibrational Structure Theory: New Vibrational Wave Function Methods for Calculation of Anharmonic Vibrational Energies and Vibrational Contributions to Molecular Properties. *Phys. Chem. Chem. Phys.* **2007**, *9*, 2942–2953.

(4) Császár, A. G. Anharmonic Molecular Force Fields. *WIREs Comput. Mol. Sci.* **2012**, *2*, 273–289.

(5) Barone, V.; Biczysko, M.; Bloino, J. Fully Anharmonic IR and Raman Spectra of Medium-Size Molecular Systems: Accuracy and Interpretation. *Phys. Chem. Chem. Phys.* **2014**, *16*, 1759–1787.

(6) Kern, C. W.; Matcha, R. L. Nuclear Corrections to Electronic Expectation Values: Zero-Point Vibrational Effects in the Water Molecule. *J. Chem. Phys.* **1968**, *49*, 2081–2091.

(7) Lounila, J.; Wasser, R.; Diehl, P. Effects of Anharmonic Vibrations on Molecular Properties. *Mol. Phys.* **1987**, *62*, 19–31.

(8) Ruud, K.; Åstrand, P.-O.; Taylor, P. R. An Efficient Approach for Calculating Vibrational Wave Functions and Zero-Point Vibrational Corrections to Molecular Properties of Polyatomic Molecules. *J. Chem. Phys.* **2000**, *112*, 2668–2683.

(9) Egidi, F.; Bloino, J.; Barone, V.; Cappelli, C. Toward an Accurate Modeling of Optical Rotation for Solvated Systems: Anharmonic Vibrational Contributions Coupled to the Polarizable Continuum Model. *J. Chem. Theory Comput.* **2012**, *8*, 585–597.

(10) Egidi, F.; Bloino, J.; Cappelli, C.; Barone, V.; Tomasi, J. Tuning of NMR and EPR parameters by vibrational averaging and environmental effects: an integrated computational approach. *Mol. Phys.* **2013**, *111*, 1345–1354.

(11) Egidi, F.; Giovannini, T.; Piccardo, M.; Bloino, J.; Cappelli, C.; Barone, V. Stereoelectronic, Vibrational, and Environmental Contributions to Polarizabilities of Large Molecular Systems: A Feasible Anharmonic Protocol. *J. Chem. Theory Comput.* **2014**, *10*, 2456–2464.

(12) Egidi, F.; Bloino, J.; Cappelli, C.; Barone, V. Development of a Virtual Spectrometer for Chiroptical Spectroscopies: The Case of Nicotine. *Chirality* **2013**, *25*, 701–708.

(13) Barone, V. The Virtual Multifrequency Spectrometer: a New Paradigm for Spectroscopy. *WIREs Comput. Mol. Sci.* **2016**, *6*, 86–110.

(14) Nielsen, H. H. The Vibration-Rotation Energies of Molecules. *Rev. Mod. Phys.* **1951**, *23*, 90–136.

(15) Clabo, D. A., Jr.; Allen, W. D.; Remington, R. B.; Yamaguchi, Y.; Schaefer, H. F., III A Systematic Study of Molecular Vibrational Anharmonicity and Vibration-Rotation Interaction by Self-Consistent-Field Higher-Derivative Methods. Asymmetric Top Molecules. *Chem. Phys.* **1988**, *123*, 187–239.

(16) Schneider, W.; Thiel, W. Anharmonic Force Fields From Analytic Second Derivatives: Method and Application to Methyl Bromide. *Chem. Phys. Lett.* **1989**, *157*, 367–373.

(17) Allen, W. D.; Yamaguchi, Y.; Cśaśzar, A. G.; Clabo, D. A.; Remington, R. B.; Schaefer, H. F., III A Systematic Study of Molecular Vibrational Anharmonicity and Vibration-Rotation Interaction by Self-Consistent-Field Higher-Derivative Methods. Linear Polyatomic Molecules. *Chem. Phys.* **1990**, *145*, 427–466.

(18) Willetts, A.; Handy, N. C.; Green, W. H., Jr.; Jayatilaka, D. Anharmonic Corrections to Vibrational Transition Intensities. *J. Phys. Chem.* **1990**, *94*, 5608–5616.

(19) Dressler, S.; Thiel, W. Anharmonic Force Fields From Density Functional Theory. *Chem. Phys. Lett.* **1997**, *273*, 71–78.

(20) Krasnoshchekov, S. V.; Isayeva, E. V.; Stepanov, N. F. Numerical-Analytic Implementation of the Higher-Order Canonical Van Vleck Perturbation Theory for the Interpretation of Medium-Sized Molecule Vibrational Spectra. *J. Phys. Chem. A* **2012**, *116*, 3691–3709.

(21) Bloino, J.; Biczysko, M.; Barone, V. General Perturbative Approach for Spectroscopy, Thermodynamics, and Kinetics: Methodological Background and Benchmark Studies. *J. Chem. Theory Comput.* **2012**, *8*, 1015–1036.

(22) Cornaton, Y.; Ringholm, M.; Ruud, K. Complete Analytic Anharmonic Hyper-Raman Scattering Spectra. *Phys. Chem. Chem. Phys.* **2016**, *18*, 22331–22342.

(23) Bloino, J.; Biczysko, M.; Barone, V. Anharmonic Effects on Vibrational Spectra Intensities: Infrared, Raman, Vibrational Circular Dichroism, and Raman Optical Activity. *J. Phys. Chem. A* **2015**, *119*, 11862−11874.

(24) Liu, J.; Liang, W. Analytical Hessian of Electronic Excited States in Time-Dependent Density Functional Theory with Tamm-Dancoff Approximation. *J. Chem. Phys.* **2011**, *135*, 014113.

(25) Liu, J.; Liang, W. Analytical Approach for the Excited-State Hessian in Time-Dependent Density Functional Theory: Formalism, Implementation, and Performance. *J. Chem. Phys.* **2011**, *135*, 184111.

(26) Petrone, A.; Lingerfelt, D. B.; Williams-Young, D. B.; Li, X. Ab Initio Transient Vibrational Spectral Analysis. *J. Phys. Chem. Lett.* **2016**, *7*, 4501−4508.

(27) Petrone, A.; Williams-Young, D. B.; Lingerfelt, D. B.; Li, X. Ab Initio Excited State Transient Raman Analysis; submitted.

(28) Williams-Young, D. B.; Scalmani, G.; Sun, S.; Frisch, M. J.; Li, X. On the Accurate and Efficient Evaluation of the Analytical Hessians of Electronically Excited States within the Random Phase Approximation; in preparation.

(29) Berger, R.; Fischer, C.; Klessinger, M. Calculation of the Vibronic Fine Structure in Electronic Spectra at Higher Temperatures. 1. Benzene and Pyrazine. *J. Phys. Chem. A* **1998**, *102*, 7157−7167.

(30) Barone, V.; Bloino, J.; Biczysko, M.; Santoro, F. Fully Integrated Approach to Compute Vibrationally Resolved Optical Spectra: From Small Molecules to Macrosystems. *J. Chem. Theory Comput.* **2009**, *5*, 540−554.

(31) Bloino, J.; Biczysko, M.; Santoro, F.; Barone, V. General Approach to Compute Vibrationally Resolved One-Photon Electronic Spectra. *J. Chem. Theory Comput.* **2010**, *6*, 1256−1274.

(32) Dierksen, M.; Grimme, S. Density Functional Calculations of the Vibronic Structure of Electronic Absorption Spectra. *J. Chem. Phys.* **2004**, *120*, 3544−3554.

(33) Dierksen, M.; Grimme, S. The Vibronic Structure of Electronic Absorption Spectra of Large Molecules: A Time-Dependent Density Functional Study on the Influence of Exact Hartree-Fock Exchange. *J. Phys. Chem. A* **2004**, *108*, 10225−10237.

(34) Avila Ferrer, F. J.; Santoro, F. Comparison of Vertical and Adiabatic Harmonic Approaches for the Calculation of the Vibrational Structure of Electronic Spectra. *Phys. Chem. Chem. Phys.* **2012**, *14*, 13549−13563.

(35) Avila Ferrer, F. J.; Cerezo, J.; Soto, J.; Improta, R.; Santoro, F. First-Principle Computation of Absorption and Fluorescence Spectra in Solution Accounting for Vibronic Structure, Temperature Effects and Solvent Inhomogenous Broadening. *Comput. Theor. Chem.* **2014**, *1040−1041*, 328−337.

(36) Gaw, J. F.; Yamaguchi, Y.; Schaefer, H. F.; Handy, N. C. Generalization of Analytic Energy Third Derivatives for the RHF Closed-Shell Wave Function: Derivative Energy and Integral Formalisms and the Prediction of Vibration-Rotation Interaction Constants. *J. Chem. Phys.* **1986**, *85*, 5132−5142.

(37) Colwell, S. M.; Jayatilaka, D.; Maslen, P. E.; Amos, R. D.; Handy, N. C. Higher Analytic Derivatives. I. A New Implementation for the Third Derivative of the SCF Energy. *Int. J. Quantum Chem.* **1991**, *40*, 179−199.

(38) Maslen, P. E.; Jayatilaka, D.; Colwell, S. M.; Amos, R. D.; Handy, N. C. Higher Analytic Derivatives. II. The Fourth Derivative of Self-Consistent-Field Energy. *J. Chem. Phys.* **1991**, *95*, 7409−7417.

(39) Ringholm, M.; Jonsson, D.; Ruud, K. A General, Recursive, and Open-Ended Response Code. *J. Comput. Chem.* **2014**, *35*, 622−633.

(40) Ringholm, M.; Jonsson, D.; Bast, R.; Gao, B.; Thorvaldsen, A. J.; Ekström, U.; Helgaker, T.; Ruud, K. Analytic Cubic and Quartic Force Fields Using Density-Functional Theory. *J. Chem. Phys.* **2014**, *140*, 034103.

(41) Bloino, J. A VPT2 Route to Near-Infrared Spectroscopy: The Role of Mechanical and Electrical Anharmonicity. *J. Phys. Chem. A* **2015**, *119*, 5269−5287.

(42) Bloino, J.; Baiardi, A.; Biczysko, M. Aiming at an Accurate Prediction of Vibrational and Electronic Spectra for Medium-to-Large Molecules: An Overview. *Int. J. Quantum Chem.* **2016**, *116*, 1543−1574.

(43) Luis, J. M.; Bishop, D. M.; Kirtman, B. A Different Approach for Calculating Franck-Condon Factors Including Anharmonicity. *J. Chem. Phys.* **2004**, *120*, 813−822.

(44) Luis, J. M.; Torrent-Sucarrat, M.; Solà, M.; Bishop, D. M.; Kirtman, B. Calculation of Franck-Condon Factors Including Anharmonicity: Simulation of the $C_2H_4^{+2}B_{3u}$ ← $C_2H_4\ \tilde{X}^1A_g$ Band in the Photoelectron Spectrum of Ethylene. *J. Chem. Phys.* **2005**, *122*, 184104.

(45) Frisch, M. J.; Trucks, G. W.; Schlegel, H. B.; Scuseria, G. E.; Robb, M. A.; Cheeseman, J. R.; Scalmani, G.; Barone, V.; Petersson, G. A.; Nakatsuji, H.; Li, X.; Caricato, M.; Marenich, A. V.; Bloino, J.; Janesko, B. G.; Gomperts, R.; Mennucci, B.; Hratchian, H. P.; Ortiz, J. V.; Izmaylov, A. F.; Sonnenberg, J. L.; Williams-Young, D.; Ding, F.; Lipparini, F.; Egidi, F.; Goings, J.; Peng, B.; Petrone, A.; Henderson, T.; Ranasinghe, D.; Zakrzewski, V. G.; Gao, J.; Rega, N.; Zheng, G.; Liang, W.; Hada, M.; Ehara, M.; Toyota, K.; Fukuda, R.; Hasegawa, J.; Ishida, M.; Nakajima, T.; Honda, Y.; Kitao, O.; Nakai, H.; Vreven, T.; Throssell, K.; Montgomery, J. A., Jr.; Peralta, J. E.; Ogliaro, F.; Bearpark, M. J.; Heyd, J. J.; Brothers, E. N.; Kudin, K. N.; Staroverov, V. N.; Keith, T. A.; Kobayashi, R.; Normand, J.; Raghavachari, K.; Rendell, A. P.; Burant, J. C.; Iyengar, S. S.; Tomasi, J.; Cossi, M.; Millam, J. M.; Klene, M.; Adamo, C.; Cammi, R.; Ochterski, J. W.; Martin, R. L.; Morokuma, K.; Farkas, O.; Foresman, J. B.; Fox, D. J. Gaussian 16, Revision A.03.; Gaussian, Inc.: Wallingford, CT, 2016.

(46) Barone, V. Anharmonic Vibrational Properties by a Fully Automated Second-Order Perturbative Approach. *J. Chem. Phys.* **2005**, *122*, 014108.

(47) Bloino, J.; Barone, V. A Second-Order Perturbation Theory Route to Vibrational Averages and Transition Properties of Molecules: General Formulation and Application to Infrared and Vibrational Circular Dichroism Spectroscopies. *J. Chem. Phys.* **2012**, *136*, 124108.

(48) Bloino, J.; Biczysko, M.; Crescenzi, O.; Barone, V. Integrated Computational Approach to Vibrationally Resolved Electronic Spectra: Anisole as a Test Case. *J. Chem. Phys.* **2008**, *128*, 244105.

(49) Egidi, F.; Bloino, J.; Cappelli, C.; Barone, V. A Robust and Effective Time-Independent Route to the Calculation of Resonance Raman Spectra of Large Molecules in Condensed Phases with the Inclusion of Duschinsky, Herzberg-Teller, Anharmonic, and Environmental Effects. *J. Chem. Theory Comput.* **2014**, *10*, 346−363.

(50) Duschinsky, F. *Acta Physicochim. URSS* **1937**, *7*, 551.

(51) Becke, A. D. Density-Functional Exchange-Energy Approximation with Correct Asymptotic Behavior. *Phys. Rev. A: At., Mol., Opt. Phys.* **1988**, *38*, 3098−3100.

(52) Becke, A. D. Density-Functional Thermochemistry. III. The Role of Exact Exchange. *J. Chem. Phys.* **1993**, *98*, 5648−5652.

(53) Lee, C.; Yang, W.; Parr, R. G. Development of the Colle-Salvetti Correlation-Energy Formula into a Functional of the Electron Density. *Phys. Rev. B: Condens. Matter Mater. Phys.* **1988**, *37*, 785−789.

(54) Dunning, T. H., Jr. Gaussian Basis Sets for Use in Correlated Molecular Calculations. I. The Atoms Boron through Neon and Hydrogen. *J. Chem. Phys.* **1989**, *90*, 1007−1023.

(55) Kendall, R. A.; Dunning, T. H., Jr.; Harrison, R. J. Electron Affinities of the First-Row Atoms Revisited. Systematic Basis Sets and Wave Functions. *J. Chem. Phys.* **1992**, *96*, 6796−6806.

(56) Woon, D. E.; Dunning, T. H., Jr. Gaussian Basis Sets for Use in Correlated Molecular Calculations. III. The Atoms Aluminum through Argon. *J. Chem. Phys.* **1993**, *98*, 1358−1371.

(57) Davidson, E. R. The Iterative Calculation of a Few of the Lowest Eigenvalues and Corresponding Eigenvectors of Real-Symmetric Matrices. *J. Comput. Phys.* **1975**, *17*, 87−94.

(58) Radziszewski, J. G.; Nimlos, M. R.; Winter, P. R.; Ellison, G. B. Infrared Absorption Spectroscopy of the Phenyl Radical. *J. Am. Chem. Soc.* **1996**, *118*, 7400−7401.

(59) Friderichsen, A. V.; Radziszewski, J. G.; Nimlos, M. R.; Winter, P. R.; Dayton, D. C.; David, D. E.; Ellison, G. B. The Infrared Spectrum of the Matrix-Isolated Phenyl Radical. *J. Am. Chem. Soc.* **2001**, *123*, 1977−1988.

(60) Butcher, V.; Costa, M.; Dyke, J.; Ellis, A.; Morris, A. A Study of the Phenyl Radical by Vacuum Ultraviolet Photoelectron Spectroscopy. *Chem. Phys.* **1987**, *115*, 261−267.

(61) Radziszewski, J. Electronic Absorption Spectrum of Phenyl Radical. *Chem. Phys. Lett.* **1999**, *301*, 565−570.

(62) Kim, G.-S.; Mebel, A. M.; Lin, S. H. Ab Initio Study of Excited Electronic States and Vibronic Spectra of Phenyl Radical. *Chem. Phys. Lett.* **2002**, *361*, 421−431.

(63) Biczysko, M.; Bloino, J.; Barone, V. First principle simulation of vibrationally resolved electronic transition of phenyl radical. *Chem. Phys. Lett.* **2009**, *471*, 143−147.

(64) Baiardi, A.; Bloino, J.; Barone, V. General Time Dependent Approach to Vibronic Spectroscopy Including Franck-Condon, Herzberg-Teller, and Duschinsky Effects. *J. Chem. Theory Comput.* **2013**, *9*, 4097−4115.

(65) Southern, C. A.; Levy, D. H.; Florio, G. M.; Longarte, A.; Zwier, T. S. Electronic and Infrared Spectroscopy of Anthranilic Acid in a Supersonic Jet. *J. Phys. Chem. A* **2003**, *107*, 4032−4040.

(66) Sobolewski, A. L.; Domcke, W. Intramolecular Hydrogen Bonding in the $S_1(\pi\pi^*)$ Excited State of Anthranilic Acid and Salicylic Acid: TDDFT Calculation of Excited-State Geometries and Infrared Spectra. *J. Phys. Chem. A* **2004**, *108*, 10917−10922.

(67) Carnimeo, I.; Puzzarini, C.; Tasinato, N.; Stoppa, P.; Charmet, A. P.; Biczysko, M.; Cappelli, C.; Barone, V. Anharmonic Theoretical Simulations of Infrared Spectra of Halogenated Organic Compounds. *J. Chem. Phys.* **2013**, *139*, 074310.

(68) Desyatnyk, O.; Pszczolkowski, L.; Thorwirth, S.; Krygowski, T. M.; Kisiel, Z. The Rotational Spectra, Electric Dipole Moments and Molecular Structures of Anisole and Benzaldehyde. *Phys. Chem. Chem. Phys.* **2005**, *7*, 1708−1715.

(69) Balfour, W. J. The Vibrational Spectrum of Anisole. *Spectrochim. Acta Part A: Mol. Spect.* **1983**, *39*, 795−800.

(70) Reddy, B. V.; Rao, G. R. Transferable Valence Force Fields for Substituted Benzenes. *Vib. Spectrosc.* **1994**, *6*, 231−250.

(71) Balfour, W. J. The 275-nm Absorption System of Anisole. *J. Mol. Spectrosc.* **1985**, *109*, 60−72.

(72) Matsumoto, R.; Sakeda, K.; Matsushita, Y.; Suzuki, T.; Ichimura, T. Spectroscopy and Relaxation Dynamics of Photoexcited Anisole and Anisole-d3 Molecules in a Supersonic Jet. *J. Mol. Struct.* **2005**, *735−736*, 153−167.

(73) Hoffmann, L. J. H.; Marquardt, S.; Gemechu, A. S.; Baumgartel, H. The Absorption Spectra of Anisole-h_8, Anisole-d_3 and Anisole-d_8. The Assignment of Fundamental Vibrations in the S_0 and the S_1 States. *Phys. Chem. Chem. Phys.* **2006**, *8*, 2360−2377.

(74) Schiccheri, N.; Pasquini, M.; Piani, G.; Pietraperzia, G.; Becucci, M.; Biczysko, M.; Bloino, J.; Barone, V. Integrated Experimental and Computational Spectroscopy Study on π-Stacking Interaction: the Anisole Dimer. *Phys. Chem. Chem. Phys.* **2010**, *12*, 13547−13554.

(75) Giuliano, B. M.; Caminati, W. Isotopomeric Conformational Change in Anisole-Water. *Angew. Chem.* **2005**, *117*, 609−612.

(76) Giuliano, B. M.; Maris, A.; Melandri, S.; Caminati, W. Pure Rotational Spectrum and Model Calculations of Anisole-Ammonia. *J. Phys. Chem. A* **2009**, *113*, 14277−14280.

(77) Pietraperzia, G.; Pasquini, M.; Mazzoni, F.; Piani, G.; Becucci, M.; Biczysko, M.; Michalski, D.; Bloino, J.; Barone, V. Noncovalent Interactions in the Gas Phase: The Anisole-Phenol Complex. *J. Phys. Chem. A* **2011**, *115*, 9603−9611.

(78) Bloino, J.; Biczysko, M.; Crescenzi, O.; Barone, V. Integrated Computational Approach to Vibrationally Resolved Electronic Spectra: Anisole as a Test Case. *J. Chem. Phys.* **2008**, *128*, 244105.

(79) Barone, V.; Bloino, J.; Biczysko, M.; Santoro, F. Fully Integrated Approach to Compute Vibrationally Resolved Optical Spectra: From Small Molecules to Macrosystems. *J. Chem. Theory Comput.* **2009**, *5*, 540−554.

(80) Bloino, J.; Baiardi, A.; Biczysko, M. Aiming at an Accurate Prediction of Vibrational and Electronic Spectra for Medium-to-Large Molecules: An Overview. *Int. J. Quantum Chem.* **2016**, *116*, 1543−1574.

(81) Ayala, P. Y.; Schlegel, H. B. Identification and Treatment of Internal Rotation in Normal Mode Vibrational Analysis. *J. Chem. Phys.* **1998**, *108*, 2314−2325.

(82) Schuurman, M. S.; Allen, W. D.; von Ragué Schleyer, P.; Schaefer, H. F., III The Highly Anharmonic BH_5 Potential Energy Surface Characterized in the Ab Initio Limit. *J. Chem. Phys.* **2005**, *122*, 104302.

(83) Bloino, J.; Barone, V. A Second-Order Perturbation Theory Route to Vibrational Averages and Transition Properties of Molecules: General Formulation and Application to Infrared and Vibrational Circular Dichroism Spectroscopies. *J. Chem. Phys.* **2012**, *136*, 124108.

(84) Liu, J.; Liang, W. Analytical Second Derivatives of Excited-State Energy within the Time-Dependent Density Functional Theory Coupled with a Conductor-Like Polarizable Continuum Model. *J. Chem. Phys.* **2013**, *138*, 024101.

(85) Zeng, Q.; Liu, J.; Liang, W. Molecular Properties of Excited Electronic State: Formalism, Implementation, and Applications of Analytical Second Energy Derivatives within the Framework of the Time-Dependent Density Functional Theory/Molecular Mechanics. *J. Chem. Phys.* **2014**, *140*, 18A506.

(86) Baiardi, A.; Bloino, J.; Barone, V. Accurate Simulation of Resonance-Raman Spectra of Flexible Molecules: An Internal Coordinates Approach. *J. Chem. Theory Comput.* **2015**, *11*, 3267−3280.

(87) Baiardi, A.; Bloino, J.; Barone, V. General Formulation of Vibronic Spectroscopy in Internal Coordinates. *J. Chem. Phys.* **2016**, *144*, 084114.

(88) Isaacson, A. D. Including Anharmonicity in the Calculation of Rate Constants. 1. The HCN/HNC Isomerization Reaction. *J. Phys. Chem. A* **2006**, *110*, 379−388.

(89) Changala, P. B.; Baraban, J. H. Ab Initio Effective Rotational and Rovibrational Hamiltonians for Non-Rigid Systems via Curvilinear Second Order Vibrational Møller-Plesset Perturbation Theory. *J. Chem. Phys.* **2016**, *145*, 174106.